

# Characterization of Nuclear Magnetism at Ultralow and Zero Field using SQUIDs

John Z. Myers, Kai Buckenmaier, Andrey N. Pravdivtsev, Markus Plaumann, and Rainer Körber

**Abstract**—Nuclear magnetism underpins areas such as medicine in magnetic resonance imaging (MRI). Hyperpolarization of nuclei enhances the quantity and quality of information that can be determined from these techniques by increasing their signal to noise ratios by orders of magnitude. However, some of these hyperpolarization techniques rely on the use of low to ultralow magnetic fields (ULF) (nTs-mTs). The broadband character and ultrasensitive field sensitivity of superconducting quantum interference devices (SQUID) allow for probing nuclear magnetism at these fields, where other magnetometers, such as Faraday coils and flux gates do not. To this end, we designed a reactor to hyperpolarize  $[1-^{13}\text{C}]$ pyruvate with the technique, signal amplification by reversible exchange in shield enables alignment transfer to heteronuclei (SABRE-SHEATH). Hyperpolarized pyruvate has been shown to be very powerful for the diagnosis of tumours with MRI as its metabolism is associated with various pathologies. We were able to characterize the field sensitivity of our setup by simulating the filled reactor in relation to its placement in our ultralow noise, ULF MRI setup. Using the simulations, we determined that our hyperpolarization setup results in a  $^{13}\text{C}$  polarization of 0.4%, a signal enhancement of  $\sim 100\,000\,000$  versus the predicted thermal equilibrium signal at earth field ( $\sim 50\ \mu\text{T}$ ). This results in a  $^{13}\text{C}$  signal of  $6.20 \pm 0.34\ \text{pT}$ , which with our ultralow noise setup, opens the possibility for direct observation of the hyperpolarization and the subsequent spin-lattice relaxation without system perturbation.

**Index Terms**—nuclear magnetism, nuclear magnetic resonance, NMR, ultralow field, zero field, SQUIDs, hyperpolarization, parahydrogen, SABRE, SABRE-SHEATH

## I. INTRODUCTION

**N**UCLEAR magnetism forms the basis behind many powerful techniques, such as magnetic resonance imaging (MRI) [1]. In the case of MRI, when nuclei of spin  $I = 1/2$  are exposed to a magnetic holding field,  $B_0$ , their two energy states ( $\alpha$  and  $\beta$ ) become nondegenerate. The difference in the number of nuclei occupying each state is described by their polarization (1) [2]:

$$P = \frac{N_\alpha - N_\beta}{N_\alpha + N_\beta} = \tanh\left(\frac{\gamma\hbar B_0}{2k_B T}\right) \quad (1)$$

where  $\gamma$  is the gyromagnetic ratio of the nuclei,  $\hbar$  the reduced Planck constant,  $T$  the temperature, and  $k_B$  the Boltzmann constant.

J.Z. Myers is with the *Physikalisch-Technische Bundesanstalt*, 10587 Berlin, Germany (email: john.myers@ptb.de). K. Buckenmaier is with the Max Planck Institute for Biological Cybernetics, 72076 Tübingen, Germany. A.N. Pravdivtsev is with the Molecular Imaging North Competence Center, 24118 Kiel, Germany. M. Plaumann is with the Otto-von-Guericke University Magdeburg, 39120 Magdeburg, Germany. R. Körber is with the *Physikalisch-Technische Bundesanstalt*, 10587 Berlin, Germany.

Manuscript received September 25, 2024; revised xxx xx, 2024.

It is this difference in occupancy of the two states that generates the nuclear magnetic moment necessary for the technique, where the signal strength is directly proportional to  $P$  [3]. At clinically relevant  $B_0$  (Ex.  $B_0 = 1.5\ \text{T}$ , polarization is on the order of ppms,  $P = 2.70\ \text{ppm}$ ) [4]. While it is enough for clinical imaging, it is far from the maximum achievable signal that could be attained from higher polarization.

Through hyperpolarization techniques, this thermal equilibrium polarization can be increased, orders of magnitude, to the order of some percent [3], [5]. One technique of interest is signal amplification by reversible exchange in shield enables alignment transfer to heteronuclei (SABRE-SHEATH), as shown in Figure 1.

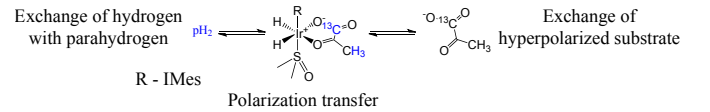


Fig. 1. Schematic of hyperpolarization of  $[1-^{13}\text{C}]$ pyruvate via SABRE-SHEATH. In blue shows the transfer of parahydrogen spin order to the  $^{13}\text{C}$  and  $^1\text{H}$  of  $[1-^{13}\text{C}]$ pyruvate.

Parahydrogen ( $\text{pH}_2$ ) is the singlet spin isomer of hydrogen, which exists as a pure state [3]. Via catalysis by an iridium based catalyst, the order of this pure state can be transferred to nuclei on another molecule, such as the preclinical probe,  $[1-^{13}\text{C}]$ pyruvate [6], [7]. This manifests as nuclear polarization, enabling metabolic imaging studies to prostate cancer diagnosis through a higher signal-to-noise ratio (SNR) [8]. However, key to this crucial polarization transfer process is a guiding field at the energy level anticrossing of the system given by (2) [9]–[11]:

$$B_{\text{LAC}} = \frac{2\pi J^{\text{HH}}}{\gamma^1\text{H} - \gamma^{13}\text{C}} \quad (2)$$

where  $J^{\text{HH}}$  is the  $J$  coupling constant between the equatorially bound hydrides on the iridium catalyst, originating from  $\text{pH}_2$  (Figure 1). Given a  $J^{\text{HH}} = -10.5\ \text{Hz}$  [12], this corresponds to a  $B_{\text{LAC}}$  of  $\sim 330\ \text{nT}$ , a field strength a full seven orders of magnitude weaker than that of a clinical MRI scanner. Therefore, optimization of the SABRE-SHEATH hyperpolarization process requires an understanding of nuclear spin physics at ultralow field (ULF).

Nuclear magnetic resonance (NMR) experiments are performed by perturbing the system either through a radio frequency pulse or field switching of the  $B_0$  field [2], [13]. The nuclear magnetic moment then precesses at a frequency proportional to its  $\gamma$  given by:  $\nu = \gamma B_0 / 2\pi$ , generating

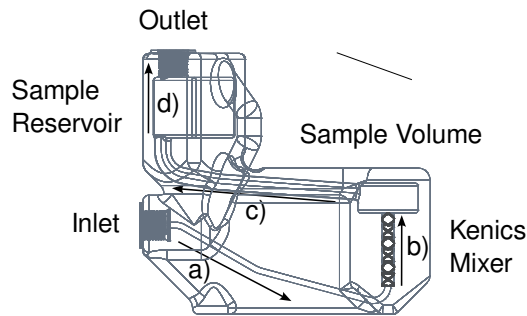


Fig. 2. Schematic of SABRE reactor. a) The capillary from the inlet to the Kenics mixer. b) The Kenics static mixer (24 mm height, 3 pairs of alternating right and left-handed helices). c) Overflow channel to the sample reservoir. d) Sample reservoir and  $pH_2$  outlet.

an oscillating magnetic signal. This signal is typically detected with a tuned Faraday coil, with its sensitivity being directly proportional to signal frequency [14]. This leads to intrinsically low system sensitivity at ULF [15]. This can be circumvented through use of a superconducting quantum interference device (SQUID). In contrast to a Faraday coil, a direct current SQUID operated in the flux locked loop mode has a field sensitivity independent of signal frequency, allowing for sensitive detection of low frequency to even nonoscillatory magnetic fields [15].

Optically pumped magnetometers (OPMs) were already used in the pioneering work of Cohen Tannoudji et al. [16] who observed the static magnetic field of hyperpolarized  $^3\text{He}$  gas. More recent OPM studies focused on detecting hyperpolarized pyruvate at ultra-low to zero field [17], investigations of its metabolic reactions [18] and the tracking of the spin dynamics of the polarization build-up during adiabatic field sweeps across the LAC condition [19] or by repeatedly inverting the polarization [20].

Based on prior work from Myers et al. [21], in this contribution we expand upon the SQUID device sensitivity and drift, demonstrating how optimizing signal enhancement obtained via SABRE-SHEATH in conjunction with an ultralow noise, ultrasensitive SQUID setup, enables the characterization of  $[1-^{13}\text{C}]$ pyruvate from ultralow down to zero field. We then show how our setup potentially enables the direct detection of nuclear magnetization without perturbation.

## II. METHODS

### A. SABRE-Reactor Design

A crucial step for the optimization of signal enhancement via SABRE-SHEATH is the recipient where hyperpolarization occurs. To this end, we designed a SABRE reactor, 3D-printed using a stereo lithography apparatus (SLA), as shown in Figure 2.  $pH_2$  enters the reactor through the inlet, which is located near the midpoint of the reactor's height. This is to minimize backflow of the liquid  $[1-^{13}\text{C}]$ pyruvate solution when  $pH_2$  gas is not flowing. After traveling through the inlet capillary (Figure 2a), the  $pH_2$  enters the static Kenics mixer (Figure 2b) [22]. The Kenics mixer covers a distance of 24 mm and is composed of three pairs of alternating single turn

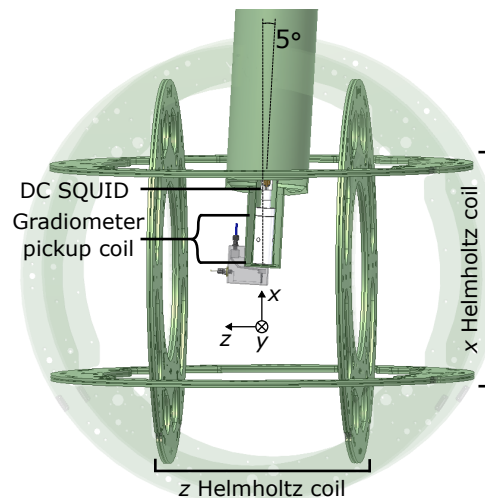


Fig. 3. Schematic of SQUID-based ULF MRI setup at the PTB. Adapted from [21].

right-handed and left-handed helices. These serve to generate turbulence between the bubbled  $pH_2$  gas and liquid sample, improving dissolution of the  $pH_2$ .

The gas then enters the principal sample volume. It is a radius  $10\text{ mm} \times 10\text{ mm}$  height cylinder, which is located directly underneath the pickup coil of the SQUID setup [21]. Afterward, the hydrogen gas leaves via an overflow channel (Figure 2c) to the sample reservoir. During bubbling,  $[1-^{13}\text{C}]$ pyruvate sample also flows through the channel into the sample reservoir, due to displacement by the  $pH_2$  gas. The channel is inclined to allow gravity to assist with backflow of  $[1-^{13}\text{C}]$ pyruvate sample back into the sample volume when  $pH_2$  is not being bubbled.

Hydrogen gas leaves the reactor setup via the outlet located vertically above the sample reservoir (Figure 2d). This serves to allow the buoyant hydrogen gas to leave, while keeping the denser liquid  $[1-^{13}\text{C}]$ pyruvate sample inside the reactor, allowing for continuous hyperpolarization of the sample.

### B. Sample Preparation

A 50 mM  $[1-^{13}\text{C}]$ pyruvate sample was prepared with 5 mM iridium 1,5-cyclooctadiene 1,3-bis(2,4,6-trimethylphenyl)imidazol-2-ylidene chloride (Ir-IMes) catalyst, and 18 mM dimethyl sulfoxide coligand in 8 mL methanol, as described in Ref. [21]. Nominally 99%  $pH_2$  was generated in a home-built  $pH_2$  generator at 25 K, based on the designs from Ref. [23]. Prior to experiments, the Ir-IMes catalyst was activated by bubbling the pyruvate solution with  $pH_2$  for half an hour at 1 standard liter per hour (sLph). During experiments,  $pH_2$  was bubbled at 2 sLph.

### C. The SQUID system

ULF NMR experiments were performed with the ULF MRI setup within the moderately, magnetically shielded room, ZUSE-MSR, at the *Physikalisch-Technische Bundesanstalt* in Berlin. A schematic of the setup is shown in Figure 3. The SABRE reactor was placed on the bottom of the ultralow

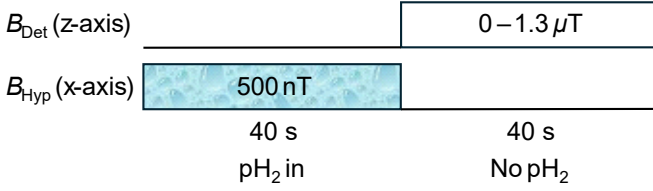


Fig. 4. Schematic of ULF NMR procedure. Acquisition was performed when  $\text{pH}_2$  was shunted.

noise, single channel SQUID system, operated in the LINOD2 liquid helium dewar [24], where the dewar with the reactor were tilted by  $5^\circ$  to aid back flow of the  $[1-^{13}\text{C}]$ pyruvate solution.

The SQUID detector was composed of a single order gradiometer pickup coil (45 mm diameter, 120 mm baseline) inductively coupled into a current-sensing SQUID, sensitive along the  $x$ -axis. Magnetic fields along the  $x$  and  $z$ -axes were generated with  $\sim 1$  m diameter Helmholtz coils.

The field sensitivity of the system was characterized by performing a 60 s acquisition at 20 kHz with the entire system in place, with no currents flowing; the acquisition was performed, during the nightly pause in train operation to minimize environmental contributions.

#### D. ULF NMR Data Acquisition and Analysis

For NMR, the  $[1-^{13}\text{C}]$ pyruvate solution was hyperpolarized via SABRE-SHEATH along the  $x$ -axis in a 500 nT hyperpolarization field ( $B_{\text{Hyp}}$ ) for 40 s. This field, higher than the  $B_{\text{LAC}}$  was used, due to rapid chemical exchange increasing the field optimum [25]. The system was then perturbed via a nonadiabatic field switch, ramping down the  $B_{\text{Hyp}}$  field and applying a perpendicular field ( $B_{\text{Det}}$ ) between  $0-1.3 \mu\text{T}$  along the  $z$ -axis. Acquisition was then performed at sample rate of 20 kHz for 40 s with  $\text{pH}_2$  being shunted away from flowing into the SABRE reactor via a three way valve (see Figure 4).

During post processing, data was baseline corrected in the time domain. To eliminate dephasing, both zeroth and first order phase correction were performed on the frequency domain of the data. The initial amplitudes of the signals attributable to the  $[1-^{13}\text{C}]$ pyruvate  $^{13}\text{C}$  were determined by applying a Lorentzian fit to the frequency domain of the data with only zeroth order phasing for each signal (more details in Ref. [21]).

#### E. Simulation of ULF NMR Spectra

The ULF NMR data was compared to theory by solving the liquid state Hamiltonian of  $[1-^{13}\text{C}]$ pyruvate, as given in (3) [21]:

$$\hat{H}^{A_3X} = -\nu^A \sum_{k=1}^3 \hat{I}_z^{A_k} - \nu^X \hat{I}_z^X + J \left( \sum_{k=1}^3 \hat{\mathbf{I}}^{A_k} \cdot \hat{\mathbf{I}}^X \right) \quad (3)$$

where  $A$  refers to  $^1\text{H}$ ,  $X$  to  $^{13}\text{C}$ , and where  $\hat{I}$  are the various product operators for the spin system and  $J$  the  $J$  coupling constant between the  $[1-^{13}\text{C}]$ pyruvate  $^{13}\text{C}$  and its  $^1\text{H}$  atoms.

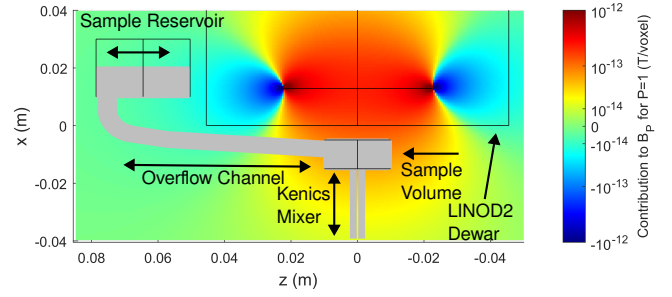


Fig. 5. Field sensitivity profile of the SQUID setup for a  $[1-^{13}\text{C}]$ pyruvate sample with 100% polarization. The filled reactor (8 mL sample with partially filled sample reservoir) is shown overlaid on the field profile.

After solving the Hamiltonian, relaxation was applied to the solution phenomenologically by multiplication with a decaying first order exponential function [21].

#### F. Determination of Sample Polarization

The polarization after hyperpolarization of  $[1-^{13}\text{C}]$ pyruvate by SABRE-SHEATH was determined by simulating the contribution of each point within the SABRE reactor to the detected signal, using the reactor and SQUID pickup loop geometries. This is possible, since SQUIDs directly detect magnetic flux, as opposed to change in magnetic flux [15]. Using the principal of reciprocity, the time dependent flux within the pickup loop was calculated as in (4) [26], [27]:

$$\Phi(t) = \mathbf{B}(\mathbf{r}) \cdot \boldsymbol{\mu}(\mathbf{r}, t) \quad (4)$$

where  $\mathbf{B}(\mathbf{r})$  is the magnetic field at point  $\mathbf{r}$ , produced by a unit current in the pick-up loop and  $\boldsymbol{\mu}(\mathbf{r}, t)$  the magnetic moment at  $\mathbf{r}$  at time  $t$ .

Assuming homogeneous hyperpolarization of the  $[1-^{13}\text{C}]$ pyruvate sample,  $\Phi(t)$  can be reformulated as flux arising from a volume element  $dV$  with magnetization  $\mathbf{M}(t)$ , as shown in (5):

$$\Phi(t) = \int_V \mathbf{B}(\mathbf{r}) \cdot \mathbf{M}(t) dV \quad (5)$$

where  $\mathbf{M}$  is related to the polarization  $\mathbf{P}$ . This is shown in equation (6) for the general case:

$$\mathbf{M} = \frac{\gamma \hbar}{2} (N_\alpha + N_\beta) \frac{\text{Tr}(\hat{\mathbf{I}}^X \hat{\rho})}{\hat{I}^X} = \frac{\gamma \hbar}{2} (N_\alpha + N_\beta) \mathbf{P} \quad (6)$$

where  $\hat{\rho}$  is the density operator. Here, non-adiabatic field switching from  $B_{\text{Hyp}}$  to  $B_{\text{Det}}$  causes  $\mathbf{M}$  and  $\mathbf{P}$  to remain along the sensor sensitive  $x$ -axis. Using the area of the pickup loop,  $A$ , the effective detected field is calculated as shown in (7):

$$B(t) = \frac{\Phi(t)}{A} = \frac{\gamma \hbar (N_\alpha + N_\beta)}{2A} \int_V \mathbf{B}(\mathbf{r}) \cdot \mathbf{P}(t) dV \quad (7)$$

$B(t)$  was then determined by discretizing the reactor volume to an isotropic 0.1 mm grid and integrating  $\Phi(t)$  numerically (Figure 5).

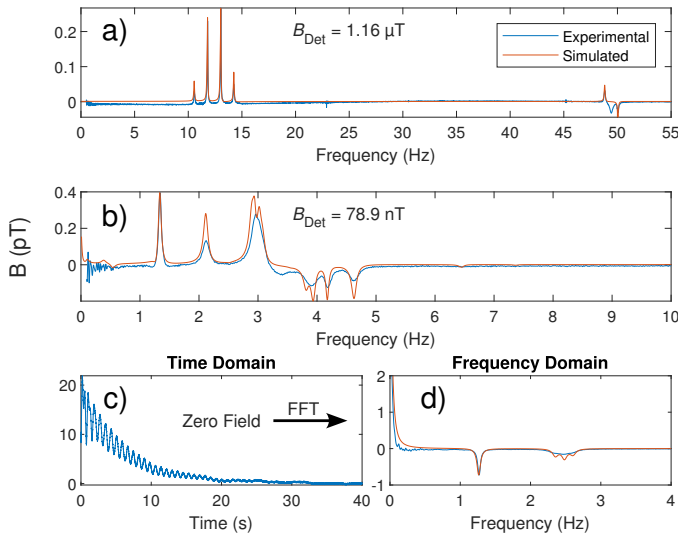


Fig. 6. Selected ULF NMR results from  $[1-^{13}\text{C}]$ pyruvate hyperpolarized via SABRE-SHEATH from [21]. Simulation parameters:  $J$  coupling constant: 1.223 Hz, ratio of  $^{13}\text{C}$  polarization to  $^1\text{H}$ : 5 000, relaxation constant:  $0.02 \text{ s}^{-1}$ . a) Spectrum from  $B_{\text{Det}} = 1.16 \mu\text{T}$ . The emissive peak at  $\sim 50$  Hz stems from hyperpolarized orthohydrogen [28], [29] which was not considered in the simulation. b) Spectrum from  $B_{\text{Det}} = 78.9 \text{ nT}$ . c) Baseline corrected time domain of zero field data. d) Spectrum at zero field.

Validity of this model was confirmed by comparison with the empirical result of the  $^1\text{H}$ -signal from an 8 mL methanol sample within the reactor. This sample was thermally polarized at 5.9 mT for 50 s, ensuring thermal equilibrium. Good agreement between the observed signal of 254 fT and the simulated signal of 275 fT was found, demonstrating how knowledge of the precise geometry of the 3D-printed reactor and SQUID detection setup allows polarimetry via simulations without the need of calibration measurements.

### III. RESULTS

#### A. Zero to ULF NMR

Selected NMR spectra from the application of our ultralow noise ULF MRI SQUID setup to the system of  $[1-^{13}\text{C}]$ pyruvate hyperpolarized by SABRE-SHEATH are shown in Figure 6. Using our setup and hyperpolarization, it was possible to characterize the NMR spectra of  $[1-^{13}\text{C}]$ pyruvate from ultralow to zero field and compare the empirical results with what was predicted from simulations. Not only did the simulations give results that agreed with the experimental data at the weak (Figure 6a) and strong coupling regimes (Figure 6d), but they also agreed with the features observed in the experimental data in the intermediate coupling regime (Figure 6b) [21].

#### B. $[1-^{13}\text{C}]$ Pyruvate Sample Polarization

Upon summing the voxels corresponding to the SABRE reactor volume in Figure 5, for a 100% polarized  $[1-^{13}\text{C}]$ pyruvate sample, the expected signal was determined to be 1.90 nT. One feature of note upon summation of the voxels is that the sample in the sample reservoir has a negative contribution to the total signal achieved. In practice, this results in a  $\sim 10\%$  decrease in the total magnetic flux from the sample in the pickup coil.

After summation of the initial amplitudes of the signals attributable to  $^{13}\text{C}$  from the hyperpolarized  $[1-^{13}\text{C}]$ pyruvate, the total  $^{13}\text{C}$  signal was determined to be  $6.20 \pm 0.34 \text{ pT}$ , yielding a total  $^{13}\text{C}$  polarization of  $\sim 0.4\%$ .

#### C. ULF MRI SQUID Setup Field Drift

A field drift of  $\sim 0.6 \text{ pT}$  was recorded by the SQUID setup over a one minute period as shown in Figure 7. In comparison to the  $6.20 \pm 0.34 \text{ pT}$  attained by SABRE-SHEATH hyperpolarization of  $[1-^{13}\text{C}]$ pyruvate, the signal was  $\sim 10$  times higher than the drift.

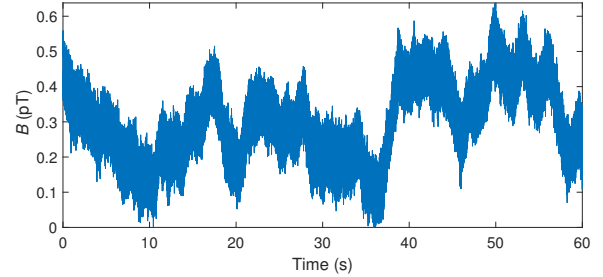


Fig. 7. Field drift of the ULF MRI SQUID setup.

### IV. DISCUSSION AND CONCLUSIONS

The application of our ultralow noise ULF MRI SQUID setup allowed for the characterization of the evolution of NMR signals from  $[1-^{13}\text{C}]$ pyruvate hyperpolarized via SABRE-SHEATH from ULF to zero field. This was made possible through the design and implementation of our home-built SABRE reactor, which used features from a static Kenics mixer to an overflow reservoir. This enabled the ability to optimize sample mixing and stabilized the sample height to maximize the attainable signal achieved from SABRE-SHEATH hyperpolarization. From this setup, we were able to attain a  $^{13}\text{C}$  signal of  $6.20 \pm 0.34 \text{ pT}$ , which upon simulation of the field contributions of the SABRE reactor, resulted in a total polarization of  $\sim 0.4\%$ . The sensitivity of our setup should allow a direct measurement of polarization build-up without any field switching or radio frequency pulses and might reveal polarization oscillations during coherent spin order transfer of the SABRE process as observed during adiabatic field ramps [19]. In addition, ULF MRI of  $^{13}\text{C}$  in  $[1-^{13}\text{C}]$ pyruvate, as demonstrated by Kempf et al. [30] could be used for future studies and optimizations of gas-fluid dynamics in the reaction chamber without susceptibility distortions.

#### ACKNOWLEDGMENTS

We would like to thank Michael Tayler and James Eills who brought to our attention previous work by Cohen-Tannoudji.

This work was funded by the DFG under Grant No. 469366436. ANP acknowledges support from the German Federal Ministry of Education and Research (BMBF) within the framework of the e:Med research and funding concept (01ZX1915C), DFG (555951950, 527469039). MOIN CC was founded by a grant from the European Regional Development Fund (ERDF) and the Zukunftsprogramm Wirtschaft of Schleswig-Holstein (Project no. 122-09-053).

## REFERENCES

- [1] R. Hashemi, W. Bradley, and C. Lisanti, *MRI: The Basics*, ser. The Basics Series. Lippincott Williams & Wilkins, 2010. [Online]. Available: <https://books.google.de/books?id=v4LFgAHXNz4C>
- [2] P. W. Atkins, *Atkins' physical chemistry*, twelfth edition ed., J. de Paula and J. J. Keeler, Eds. Oxford: Oxford University Press, 2023, Hinweis: Zugang zu allen Online-Inhalten und -Materialien erhält der Käufer ausschließlich für den eigenen, privaten Gebrauch. Nutzung durch Bibliotheken, Institute und Lehr-Einrichtungen ist nicht erlaubt.
- [3] R. A. Green, R. W. Adams, S. B. Duckett, R. E. Mewis, D. C. Williamson, and G. G. Green, "The theory and practice of hyperpolarization in magnetic resonance using parahydrogen," *Progress in Nuclear Magnetic Resonance Spectroscopy*, vol. 67, pp. 1–48, 2012. [Online]. Available: <https://www.sciencedirect.com/science/article/pii/S0079656512000477>
- [4] R. R. Edelman, "The history of mr imaging as seen through the pages of radiology," *Radiology*, vol. 273, no. 2S, pp. S181–S200, Nov. 2014.
- [5] J. H. Ardenkjær-Larsen, B. Fridlund, A. Gram, G. Hansson, L. Hansson, M. H. Lerche, R. Servin, M. Thaning, and K. Golman, "Increase in signal-to-noise ratio of  $\zeta$  10,000 times in liquid-state NMR," *Proceedings of the National Academy of Sciences*, vol. 100, no. 18, pp. 10 158–10 163, aug 2003.
- [6] W. Iali, S. S. Roy, B. J. Tickner, F. Ahwal, A. J. Kennerley, and S. B. Duckett, "Hyperpolarising pyruvate through signal amplification by reversible exchange (SABRE)," *Angewandte Chemie International Edition*, vol. 58, no. 30, pp. 10 271–10 275, jul 2019.
- [7] C. H. Cunningham, J. Y. Lau, A. P. Chen, B. J. Geraghty, W. J. Perks, I. Roifman, G. A. Wright, and K. A. Connelly, "Hyperpolarized  $^{13}\text{C}$  metabolic mri of the human heart: Initial experience," *Circulation Research*, vol. 119, no. 11, pp. 1177–1182, Nov. 2016.
- [8] M. J. Albers, R. Bok, A. P. Chen, C. H. Cunningham, M. L. Zierhut, V. Y. Zhang, S. J. Kohler, J. Tropp, R. E. Hurd, Y.-F. Yen, S. J. Nelson, D. B. Vigneron, and J. Kurhanewicz, "Hyperpolarized  $^{13}\text{C}$  Lactate, Pyruvate, and Alanine: Noninvasive Biomarkers for Prostate Cancer Detection and Grading," *Cancer Research*, vol. 68, no. 20, pp. 8607–8615, 10 2008.
- [9] A. N. Pravdivtsev, A. V. Yurkovskaya, H.-M. Vieth, K. L. Ivanov, and R. Kaptein, "Level anti-crossings are a key factor for understanding para-hydrogen-induced hyperpolarization in SABRE experiments," *ChemPhysChem*, vol. 14, no. 14, pp. 3327–3331, aug 2013.
- [10] T. Theis, M. L. Truong, A. M. Coffey, R. V. Shchepin, K. W. Waddell, F. Shi, B. M. Goodson, W. S. Warren, and E. Y. Chekmenev, "Microtesla sabre enables 10% nitrogen-15 nuclear spin polarization," *Journal of the American Chemical Society*, vol. 137, no. 4, pp. 1404–1407, 2015, pMID: 25583142.
- [11] K. L. Ivanov, A. N. Pravdivtsev, A. V. Yurkovskaya, H.-M. Vieth, and R. Kaptein, "The role of level anti-crossings in nuclear spin hyperpolarization," *Progress in Nuclear Magnetic Resonance Spectroscopy*, vol. 81, pp. 1–36, aug 2014.
- [12] C. D. Assaf, X. Gui, A. A. Auer, S. B. Duckett, J.-B. Hövener, and A. N. Pravdivtsev, "J coupling constants of  $\zeta$  1 hz enable  $^{13}\text{C}$  hyperpolarization of pyruvate via reversible exchange of parahydrogen," *The Journal of Physical Chemistry Letters*, vol. 15, no. 5, pp. 1195–1203, Jan. 2024.
- [13] D. A. Barskiy, J. W. Blanchard, D. Budker, J. Eills, S. Pustelny, K. F. Sheberstov, M. C. D. Tayler, and A. H. Trabesinger, "Zero- to ultralow-field nuclear magnetic resonance," Aug. 2024.
- [14] M. H. Levitt, *Spin dynamics: basics of nuclear magnetic resonance*. Wiley, 2008. [Online]. Available: <https://eprints.soton.ac.uk/27761/>
- [15] W. Myers, D. Slichter, M. Hatridge, S. Busch, M. Möble, R. McDermott, A. Trabesinger, and J. Clarke, "Calculated signal-to-noise ratio of MRI detected with SQUIDs and Faraday detectors in fields from  $10\mu\text{T}$  to 1.5T," *Journal of Magnetic Resonance*, vol. 186, no. 2, pp. 182–192, jun 2007.
- [16] C. Cohen-Tannoudji, J. DuPont-Roc, S. Haroche, and F. Laloë, "Detection of the static magnetic field produced by the oriented nuclei of optically pumped  $\text{He}^3$  gas," *Physical Review Letters*, vol. 22, no. 15, pp. 758–760, Apr. 1969.
- [17] A. Ortmeier, K. MacCulloch, D. A. Barskiy, N. Kempf, J. Z. Myers, R. Körber, A. N. Pravdivtsev, K. Buckenmaier, and T. Theis, "Sabre-hyperpolarization dynamics of  $[1-^{13}\text{C}]$ pyruvate monitored by in situ zero- to ultra-low field nmr," *Journal of Magnetic Resonance Open*, vol. 19, p. 100149, Jun. 2024.
- [18] J. Eills, R. Picazo-Frutos, O. Bondar, E. Cavallari, C. Carrera, S. J. Barker, M. Utz, A. Herrero-Gómez, I. Marco-Rius, M. C. D. Tayler, S. Aime, F. Reineri, D. Budker, and J. W. Blanchard, "Enzymatic reactions observed with zero- and low-field nuclear magnetic resonance," *Analytical Chemistry*, vol. 95, no. 49, pp. 17 997–18 005, Dec. 2023.
- [19] J. Eills, M. W. Mitchell, I. M. Rius, and M. C. D. Tayler, "Live magnetic observation of parahydrogen hyperpolarization dynamics," *Proceedings of the National Academy of Sciences*, vol. 121, no. 43, Oct. 2024.
- [20] K. Mouloudakis, S. Bodenstedt, M. Azagra, M. W. Mitchell, I. Marco-Rius, and M. C. Tayler, "Real-time polarimetry of hyperpolarized  $^{13}\text{C}$  nuclear spins using an atomic magnetometer," 2023.
- [21] J. Z. Myers, F. Bullinger, N. Kempf, M. Plaumann, A. Ortmeier, T. Theis, P. Povolni, J. Romanowski, J. Engelmann, K. Scheffler, J.-B. Hövener, K. Buckenmaier, R. Körber, and A. N. Pravdivtsev, "Zero to ultralow magnetic field NMR of  $[1-^{13}\text{C}]$ pyruvate and  $[2-^{13}\text{C}]$ pyruvate enabled by SQUID sensors and hyperpolarization," *Physical Review B*, vol. 109, no. 18, p. 184443, May 2024.
- [22] D. Hobbs and F. Muzzio, "The kenics static mixer: a three-dimensional chaotic flow," *Chemical Engineering Journal*, vol. 67, no. 3, pp. 153–166, Jun. 1997.
- [23] K. Buckenmaier, M. Rudolph, C. Back, T. Misztal, U. Bommerich, P. Fehling, D. Koelle, R. Kleiner, H. A. Mayer, K. Scheffler, J. Bernarding, and M. Plaumann, "SQUID-based detection of ultra-low-field multinuclear NMR of substances hyperpolarized using signal amplification by reversible exchange," *Scientific Reports*, vol. 7, no. 1, oct 2017.
- [24] J.-H. Storm, P. Hömmen, D. Drung, and R. Körber, "An ultra-sensitive and wideband magnetometer based on a superconducting quantum interference device," *Appl. Phys. Lett.*, vol. 110, no. 7, p. 072603, Feb. 2017.
- [25] R. W. Adams, J. A. Aguilar, K. D. Atkinson, M. J. Cowley, P. I. P. Elliott, S. B. Duckett, G. G. R. Green, I. G. Khazal, J. López-Serrano, and D. C. Williamson, "Reversible interactions with para-hydrogen enhance NMR sensitivity by polarization transfer," *Science*, vol. 323, no. 5922, pp. 1708–1711, mar 2009.
- [26] D. Hoult and P. C. Lauterbur, "The sensitivity of the zeugmatographic experiment involving human samples," *Journal of Magnetic Resonance (1969)*, vol. 34, no. 2, pp. 425–433, may 1979.
- [27] K. Buckenmaier, A. Pedersen, P. SanGiorgio, K. Scheffler, J. Clarke, and B. Inglis, "Feasibility of functional mri at ultralow magnetic field via changes in cerebral blood volume," *NeuroImage*, vol. 186, pp. 185–191, Feb. 2019.
- [28] D. A. Barskiy, K. V. Kovtunov, I. V. Koptug, P. He, K. A. Groome, Q. A. Best, F. Shi, B. M. Goodson, R. V. Shchepin, A. M. Coffey, K. W. Waddell, and E. Y. Chekmenev, "The feasibility of formation and kinetics of NMR signal amplification by reversible exchange (SABRE) at high magnetic field (9.4 t)," *Journal of the American Chemical Society*, vol. 136, no. 9, pp. 3322–3325, feb 2014.
- [29] K. Buckenmaier, K. Scheffler, M. Plaumann, P. Fehling, J. Bernarding, M. Rudolph, C. Back, D. Koelle, R. Kleiner, J.-B. Hövener, and A. N. Pravdivtsev, "Multiple quantum coherences hyperpolarized at ultra-low fields," *ChemPhysChem*, vol. 20, no. 21, pp. 2823–2829, oct 2019.
- [30] N. Kempf, R. Körber, M. Plaumann, A. N. Pravdivtsev, J. Engelmann, J. Boldt, K. Scheffler, T. Theis, and K. Buckenmaier, " $^{13}\text{C}$  mri of hyperpolarized pyruvate at  $120\mu\text{T}$ ," *Scientific Reports*, vol. 14, no. 1, Feb. 2024.